

Insertion of Lithium Ions into Carbon Nanotubes: An ab Initio Study

Tapas Kar,* Jayasree Pattanayak, and Steve Scheiner

Department of Chemistry and Biochemistry, Utah State University, Logan, Utah 84322-0300

Received: May 4, 2001; In Final Form: August 23, 2001

Theoretical investigations have been carried out to explore the possibilities of Li⁺ ion intercalation or insertion through the side-wall or through the cap region of carbon nanotubes. Hartree–Fock(HF), MP2 and density functional (DFT) theories with minimal to extended basis sets were used to examine simple models of 5, 6, 7, and eight-membered-rings. The barrier to insert Li⁺ ion through these rings depends on the ring size. Insertion is easier as the ring size increases. Lithium ion favors two positions: (a) inside the tube close to the wall, and (b) outside of the tube. Energetic information is provided using simple models with different diameters. Movement of the cation(s) within a single-wall tube, in interstitial zone and within multiwall tube, are also studied and discussed.

Introduction

Lithium metal is the most powerful reducing element. It has the lowest electronegativity and standard cell potential of -3.045 V of all metals. When associated with strong oxidants such as MnO₂, V₂O₅, etc. lithium leads to high voltage and high energy batteries. Because of small size, lightweight, and high energy density, Li batteries have applications requiring higher and higher energy density for power source over other conventional batteries, like, Pb, Ni–Cd, and Ni–MH.^{1,2} However, dendritic formation (which causes low cycle life and poor safety aspects³) on the surface of negative electrode of Li metal during charge/discharge process currently restricts it to secondary cell applications. To avoid this dendritic behavior of Li metal electrode, a “rocking-chair” concept has been established, in which the intercalation phenomenon has been used as an anode reaction for lithium secondary batteries.^{4–6}

Although lithium intercalated into a carbon matrix has been an interesting topic of electrochemistry over the years, the importance of such materials gained renewed attention after breakthrough news in battery history from Sony in 1990.⁷ The company announced the commercialization of Li ion rechargeable batteries, where metallic lithium is replaced by a carbon host structure. Such material has the very special characteristics that it can reversibly absorb and release Li ions at low electrochemical potentials. Use of such a battery has the advantage of much improved cycle life and safety over lithium battery.

Of the various forms of carbon, graphite is the best host material to reversibly intercalate lithium, and such systems are termed graphite intercalation compounds (GICs). The limit for graphite under ambient conditions is one lithium atom per six C atoms, which results in a specific capacity of 372 mA/g. So far, various (natural and artificial^{8,9}) types of carbon materials (GICs) and electrolytes have been investigated and two recent review articles^{10,11} summarize those investigations.

Besides artificially prepared graphites, different doping agents have also been explored in Li ion battery research. Dahn and co-workers¹² reported larger reversible specific capacities (>500 mA/g) and good cycling stability in high hydrogen-concentrating (H/C atomic ratio > 0.05) carbons. Even higher

capacity (~ 700 mA/g) has been found^{13,14} in poly(*p*-phenylene) (PPP) based polymeric carbons at 700 °C. Several conducting polymers such as polyaniline, polypyrrole, and polythiophene are promising anode materials because they are stable in air and have good electrochemical properties.¹⁵

Superdense Li-GICs (LiC₄, LiC₂) have also been synthesized^{16–18} by compressing powder of lithium metal with highly oriented pyrolytic graphite (HOPG) under high pressure. The specific capacity is about three times (~ 900 mA/g) greater than the ideal 372 mA/g value. Unfortunately, such dense carbon materials with high specific capacity are thermodynamically unstable at ambient pressure, and decompose slowly to well-defined LiC₆ + Li metal.

Although several carbon fiber materials have been tested for improved Li ion batteries, a new direction has opened in battery research after the discovery of carbon nanotubes (CNTs)¹⁹ because of completely different intercalation sites, i.e., between the pseudographic layers, interstitial sites or inside the tubes (capillary effects) etc. The different electrical properties of CNTs, depending on their diameter, length and chirality, also lead to the belief that lithium intercalated CNTs are highly promising. Two types of CNTs, namely, multiwall carbon nanotubes (MWNTs) and single-wall nanotubes (SWNTs), can now be easily synthesized.^{20–25} Both types of CNTs have recently been considered experimentally and theoretically^{26–30} as anode materials. However, studies on Li intercalation/insertion in CNTs are in their infancy.

Lithium intercalation in CNTs under high-pressure conditions in argon atmosphere were studied and characterized by Nalimova et al.²⁶ The IR spectra of the doped nanotube observed in the 450–690 cm⁻¹ region are similar to the bands found in Li-GICs. The possibility of lithium intercalation inside the nanotube channels was not confirmed or rejected by the IR data. Electrochemical intercalation in SWNTs²⁷ and MWNTs^{28,29} has also been reported recently. These investigations confirmed the presence of lithium in CNTs, and the specific capacity is higher than that of Li-GICs. Gao et al.^{27,31} used SWNTs synthesized by laser ablation for electrochemical intercalation of lithium. They showed that SWNTs have substantially higher reversible Li capacity than do graphite and MWNTs. X-ray diffraction (XRD), ⁷Li NMR, and transmission electron microscopic (TEM) data²⁸ on capped Li-MWNTs support the presence of lithium

* To whom correspondence should be addressed. E-mail: tapaskar@cc.usu.edu.

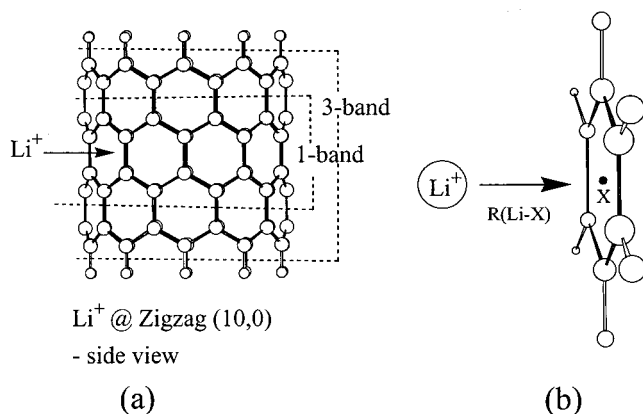


Figure 1. Insertion of Li^+ into 1-band and 3-band carbon nanotubes (a), and into benzene ring (b).

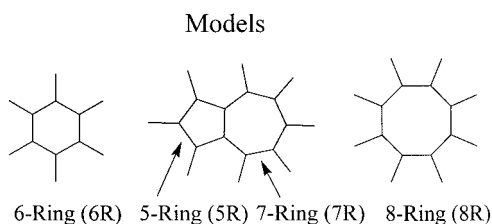


Figure 2. Simple ring models.

ions in CNTs as swelling zones (as in a necklace of pearls) in intercalated tubes. The tubular morphology (except for some rupture on the wall of the tube) and the diameter of the capped tube have not changed after Li has been deintercalated. On the basis of these results, Maurin et al.²⁸ predict that insertion/intercalation takes place through the side-wall of the nanotubes.

Although experimental evidence suggests several possible Li intercalated carbon single and multiwalled nanotubes, the positions of lithium in tubes have not been determined. It is also unclear how lithium ions get inside the single-walled tubes or bundle of SWNT, and which side (inside the capillary or outside) of the SWNT is preferable for lithium. All these questions are answerable by theoretical calculations. With this objective in mind we have undertaken a thorough theoretical investigation in order to understand the Li ion intercalation process, and the structure and stability of Li^+ @ CNTs.

Method of Calculations. Because of the large size of carbon nanotubes highly accurate ab initio theoretical calculations of the full system are impractical. One might consider lower level of theories but the accuracy and reliability of the results would be questionable. A reasonable compromise would involve construction of a good model with fewer atoms, but one which mimics the actual system. One can then apply accurate and reliable theoretical methods and have a measure of confidence in the results. It is the latter approach which we adopt here.

Carbon nanotubes are composed largely of many hexagons, and intercalation or insertion of Li ions takes place through those rings as shown in Figure 1a. The process of insertion of Li^+ through the side-wall of the tube can be simplified by considering a benzene molecule, as shown in Figure 1b. In this model, lithium ion passes through the center of the benzene ring. In addition to hexagons, pentagons and heptagons are also present in nanotubes, in their junctions, and in the capped zone of the closed tube.²⁰ Considering all possible rings in nanotubes, several simple models were selected as shown in Figure 2.

In addition to pentagon (5R), hexagon (6R), and heptagon (7R) rings, an octagon (8R) (as higher structural defect in nanotubes) was also included in the model list. It may be noted

TABLE 1: Li^+ (6R) Binding Energies (ΔE) and the Equilibrium Distances $R(\text{LiX})$ between Li^+ and the Center X of the 6R as Shown in Figure 1b

| methods | ΔE^a , eV | $R(\text{LiX})$, Å |
|----------------------|-------------------|---------------------|
| HF/STO-3G | -3.69 | 1.713 |
| HF/3-21G | -1.90 | 1.949 |
| HF/6-31G* | -1.76 | 1.942 |
| MP2/STO-3G | -3.97 | 1.697 |
| MP2/3-21G | -1.95 | 1.928 |
| MP2/6-31G* | -1.90 | 1.921 |
| DFT-B3LYP/STO-3G | -3.42 | 1.732 |
| DFT-B3LYP/3-21G | -2.02 | 1.883 |
| DFT-B3LYP/6-31G* | -1.84 | 1.880 |
| HF/6-311++G** | -1.66 | 1.885 |
| MP2/6-311++G** | -1.67 | 1.868 |
| DFT-B3LYP/6-311++G** | -1.67 | 1.841 |

$$^a \Delta E = E(\text{Li}^+ @ 6\text{R}) - E(6\text{R}) - E(\text{Li}^+).$$

that individual 5R and 7R (with appropriate number of hydrogen atoms) are open-shell molecules, so they are not representative of the nanotubes. The alternative singly charged closed-shell C_5H_5 and C_7H_7 ions are also not an appropriate model because of the extra atomic charge. To circumvent these problems, we considered attached 5 and 7 ring systems as shown in Figure 2, which together comprises a closed-shell molecule.

Initial calculations on these simple models have been carried out using HF, MP2, and DFT-B3LYP methods. A wide range of basis sets from minimal to extended, namely, STO-3G, 3-21G, 6-31G*, and 6-311++G**, has been used. To assess the reliability of model calculations, lithium ion intercalation into two different zigzag (10,0) nanotubes with different lengths has also been studied. These nanotubes are referred to as 1-band and 3-band as shown in Figure 1a. All calculations have been performed using the Gaussian98A7 program package.³²

Results and Discussion

Model Systems. The interaction between lithium ion and benzene (6R) is a well-known cation- π interaction that has been studied thoroughly by high level ab initio methods^{33,34} and experimentally.³⁵ In general, binding energies and distances between metal cations (Li^+ , Na^+ , K^+ , etc) and π systems (like C_2H_2 , C_2H_4 , benzene etc.) depend strongly on the method and basis functions.^{33,36}

The electronic binding energies (ΔE) of Li^+ (6R) calculated at different levels of theory are summarized in Table 1. Geometries are optimized at each level of theory. It may be noted that the hydrogen atoms of $\text{C}_6\text{H}_6\text{Li}^+$ are tilted slightly (less than 0.5°) out of the benzene plane, in the opposite direction from the approaching lithium ion. This sort of geometric distortion has also been found in other cation- π systems.^{36,37} The third column of Table 1 contains the optimized Li-X (X is the center of the ring, as shown in Figure 1b) distances. Energy values obtained from the highest level of calculations using 6-311++G** basis sets are in good agreement with the experimental binding energy³³ of 1.70 ± 0.14 eV.

In general, HF, MP2, and DFT energies are close to one another. Compared to 6-311++G** results, STO-3G energies are higher by a factor of more than two, and 3-21G and 6-31G* values are within 1.1 to 1.2 of the MP2/6-311++G** energy. The STO-3G $R(\text{LiX})$ distances are out of the range of 1.84 to 1.95 Å, obtained for 3-21G and higher basis sets of the present and previous investigations.³³⁻³⁵

The energy associated with moving the lithium ion along an axis perpendicular to the benzene is shown in Figure 3. First-principles study³⁰ on Li-intercalated carbon nanotube ropes indicated small structural deformation due to intercalation. The

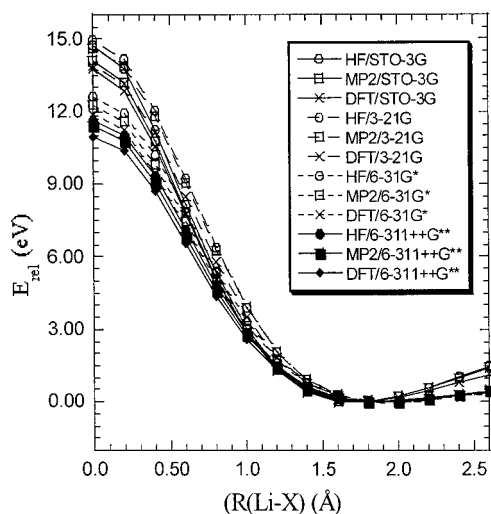


Figure 3. Variation of energies by moving lithium ion from 2.6 Å to the center (X) of the 6-ring.

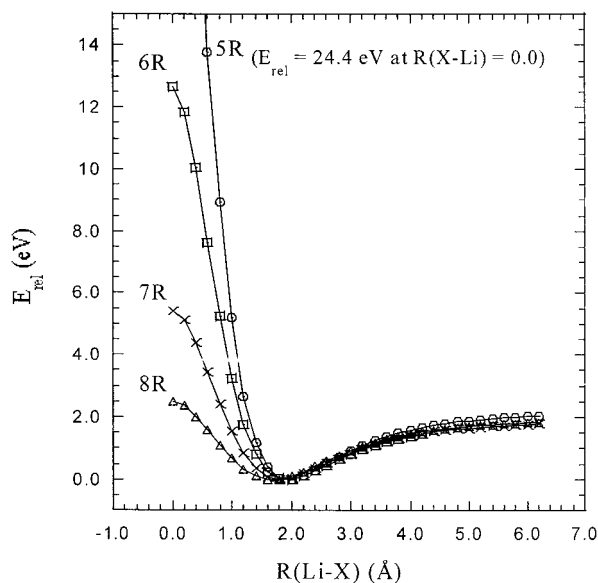


Figure 4. Variation of MP2/6-31G* energies by moving lithium ion from 6.0 Å to the center (X) of the 5, 6, 7, and 8-rings.

CC distances of 6R were kept fixed at 1.4 Å, which is the typical CC bond length found in carbon nanotubes. The hydrogen atoms were also restricted to the benzene ring plane. It can be seen that all methods and basis functions predict a minimum around 1.8 Å from the center of the ring. As Li⁺ moves toward the center of the ring, the energies rise sharply, and reach a maximum in the ring plane. Thus, the lithium ion would have to cross an exceedingly high energy barrier to enter the tube through the hexagons of the side-wall or cap-region of the tube. This barrier is estimated to lie in the range between 11 and 15 eV, depending on the particular theoretical method.

The next step considered different sizes of the ring. The Li⁺ ion is slowly brought to the center (X) of the 5R, 7R, and 8R of Figure 2 from a distance of 6 Å. In each case, X represents the center of the appropriate ring. The geometries of the rings were kept fixed at their optimized values. MP2/6-31G* potential energy surfaces thus obtained for different rings are shown in Figure 4, along with the corresponding PES of 6R. (All other methods and basis sets produce similar PES curves, except slightly different barrier heights.) The intercalation energy is lowered drastically from 24 eV to about 2 eV as the ring

TABLE 2: Energy (in eV) Required to Push Li⁺ through the Center of Different Rings

| | fixed ring geometry | | | |
|------------|--------------------------|------|-----|------|
| | 5R | 6R | 7R | 8R |
| HF/6-31G* | 23.2 | 11.6 | 4.4 | 1.2 |
| MP2/6-31G* | 22.2 | 10.8 | 3.5 | 0.6 |
| DFT/6-31G* | 21.3 | 10.4 | 3.5 | 0.5 |
| | fully optimized geometry | | | |
| | 5R | 6R | 7R | 8R |
| HF/6-31G* | 15.6 | 8.6 | 3.5 | 0.9 |
| MP2/6-31G* | 13.8 | 7.4 | 2.6 | 0.01 |
| DFT/6-31G* | 13.4 | 7.4 | 2.6 | 0.22 |

TABLE 3: Binding Energies and Equilibrium LiX^a Distances

| | energies (eV) | | | |
|------------|---------------|-------|-------|-------|
| | 5R | 6R | 7R | 8R |
| HF/6-31G* | -2.23 | -1.76 | -1.65 | -1.49 |
| MP2/6-31G* | -2.21 | -1.90 | -1.92 | -1.13 |
| DFT/6-31G* | -2.22 | -1.84 | -1.79 | -1.54 |
| | distances (Å) | | | |
| | 5R | 6R | 7R | 8R |
| HF/6-31G* | 1.934 | 1.942 | 1.880 | 1.761 |
| MP2/6-31G* | 1.944 | 1.921 | 1.807 | 1.661 |
| DFT/6-31G* | 1.898 | 1.880 | 1.778 | 1.638 |

^a X is the center of each of the rings.

size increases from 5 to 8. The insertion process in carbon nanotubes is thus predicted to become progressively easier as the structural defect become higher. This finding is confirmed by surmises by Maurin et al.²⁸ based on their recent experimental studies.

Additional calculations were performed to estimate insertion/intercalation energies when ring geometries are allowed to relax. These barriers at fixed and relaxed ring geometries are summarized in Table 2, where it may be seen that energy barriers are lowered when the rings are allowed to expand. The lengthening of the CC distances decrease with the increasing size of the rings. In fact one of the CC bonds in 5R becomes longer than 2 Å during the insertion process. The minimum distortion of 0.04 Å is found in 8R where the change of barrier height is also the lowest out of the four rings.

It was shown above in Figure 4, that the Li-X equilibrium distance of 1.8 Å is virtually independent of the size of the rings. Table 3 summarizes the electronic binding energies and equilibrium LiX distances obtained from full optimizations. As mentioned earlier, these quantities depend on the method of calculation. In general, the binding energy diminishes with increasing ring size, and the distance between the cation and π -systems follows the same trend.

In conclusion, passage of the Li⁺ ion through the center of a ring is much easier for larger rings. Allowing the ring to deform facilitates the passage, especially for small rings.

Two Six-Ring Model. The intercalation of lithium ion with a single ring can serve as a first approximation to potential experienced by the ion outside of the nanotube. An analogous approximation for the ion inside the tube is illustrated in Figure 5a. This two 6R model can be considered as the interaction between Li⁺ and the hexagons on the opposite walls of a single-wall nanotube, where distance L between these two rings corresponds to the diameter of the tube. The same model can refer to the hexagons of two nanotubes of a bundle at an interlayer distance of L .

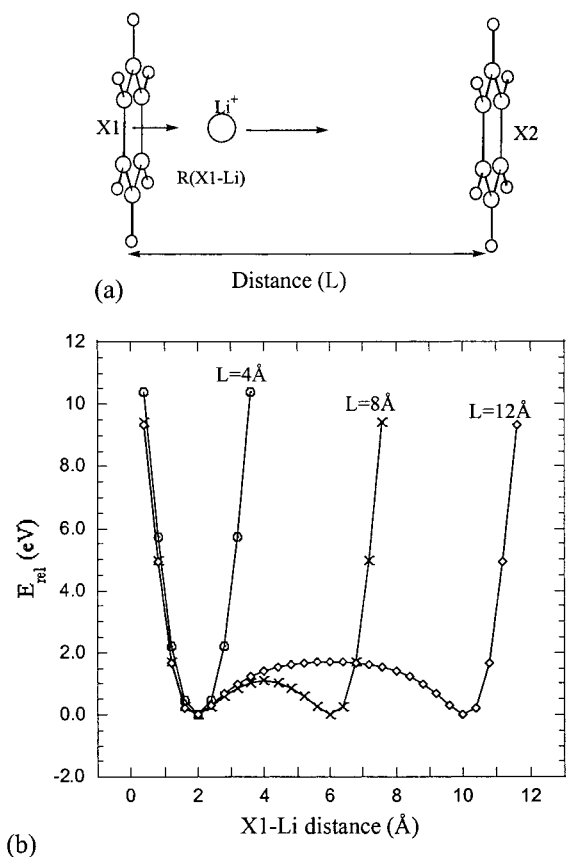


Figure 5. Two 6-ring model where L is the distance between two benzene molecules (a). Variation of energies (MP2/6-31G*) by moving lithium ion between two benzene molecules (b).

TABLE 4: Barrier Heights (eV) at Different L of Figure 5

| methods | $L = 8 \text{ \AA}$ | | $L = 12 \text{ \AA}$ | | $L = 24 \text{ \AA}$ |
|-----------|---------------------|--------|----------------------|--------|----------------------|
| | 3-21G | 6-31G* | 3-21G | 6-31G* | 6-31G* |
| HF | 1.04 | 0.98 | 1.71 | 1.60 | 1.81 |
| MP2 | 1.02 | 1.08 | 1.69 | 1.69 | 1.90 |
| DFT-B3LYP | 1.10 | 1.04 | 1.77 | 1.63 | 1.83 |

The energies obtained by moving the ion from the center of the left ring (X1) to the center of the right 6R (X2) are shown in Figure 5b. Three different diameters of the nanotubes (or inter-tube spacing between two tubes) are illustrated. At $L = 4 \text{ \AA}$, all three methods, namely, HF, MP2, and DFT-B3LYP indicate a single well potential in which the ion strongly prefers its equilibrium position at the center of the tube. Hence, tubes with such small diameter (or interstitial distance) will not be a good choice for Li ion rechargeable battery. At longer L , the Li^+ crosses through two minima around 2 \AA from each ring, and a barrier is encountered equidistant from the two rings. The barrier height (E^\ddagger) increases as the two rings are further separated. For example, the MP2/6-31G* value of E^\ddagger at $L = 8 \text{ \AA}$ is 1.08 eV, which goes up to 1.69 eV at $L = 12 \text{ \AA}$ and 1.90 eV for $L = 24 \text{ \AA}$ (not shown here). This increasing trend in E^\ddagger with L is independent of the method and basis set (see Table 4). Thus, it seems that the difficulty of movement of lithium ions within the tubes (or between two tubes) strongly depends on their diameters (or intertube distances in bundle of tubes).

1-Band and 3-Band Carbon Nanotubes. The reliability of the results obtained using simple ring models may be tested by considering actual carbon nanotubes. For purposes of examining the lithium insertion process through the side-wall of the tube, the length of the tube is not expected to be an important factor.

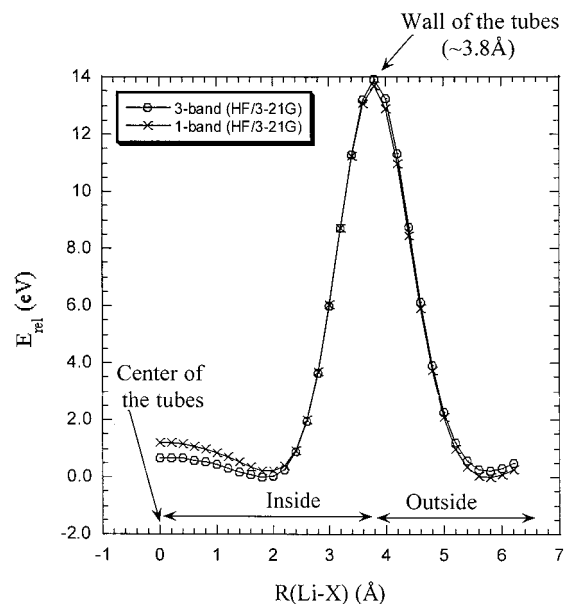


Figure 6. Variation of energies by moving lithium ion from outside to the center (X) of 1-band and 3-band carbon nanotubes.

This expectation may be tested by comparing two small tubes with different lengths but same diameter. These nanotubes, as shown in Figure 1a, are referred to as 1-band and 3-band zigzag (10,0) nanotubes, or simply 1-band and 3-band tubes, respectively. Both these tubes are constituted of hexagons (6R model).

The HF/3-21G energies obtained by moving lithium ion from outside to the center (X) of those tubes, through the side-wall, are shown in Figure 6. As the ion approaches the tube, it passes through a minimum around 5.8 \AA before reaching the maximum at the wall. Because the tube radius is close to 4 \AA , this minimum lies about 1.8 \AA from the wall, quite similar to the position of the minimum in Figure 3 for the simpler system 6R. The barrier heights of $\sim 14.0 \text{ eV}$ obtained in these 1 and 3-band tubes are also close to the benzene result (14.7 eV at HF/3-21G level).

Once the cation crosses the high barrier at the wall, the energy drops sharply to the second minimum, located around 2 \AA from the wall of the tube. Further pushing the ion toward the center of the tube causes a slight increase in energy and finally a second maximum. Thus, the movement of Li^+ inside the tube from one wall to the opposite wall passes through an energy barrier. Interestingly, this barrier height (E^\ddagger) depends on the length of the tubes. The E^\ddagger value of 1.2 eV drops to 0.7 eV with the extension of the tube from 1-band to 3-band. On the other hand, the higher barrier, at the tube wall, is quite insensitive to the tube length.

One can also examine the validity of the two 6-ring model, as described in Figure 5b and discussed in the previous section. Because the diameters of both 1-band and 3-band tubes (Figure 1a) are close to 8 \AA , Figure 5b with $L = 8 \text{ \AA}$ may be fairly compared to the “inside” part of the PES curve in Figure 6. The nature of the curves is similar for both the small model and actual tubes. The HF/3-21G barrier height of 1.02 eV at the center of the model is in good agreement with that of the 1-band tube.

We also verified the results obtained from our two 6R model by considering two tubes at a distance of 8 \AA , as shown in Figure 7a. The corresponding HF/3-21G PES curve is shown in Figure 7b. It can be seen the nature of this curve is the same as the model: a minimum around 2 \AA from the wall of left tube, and the barrier height is about 1.2 eV .

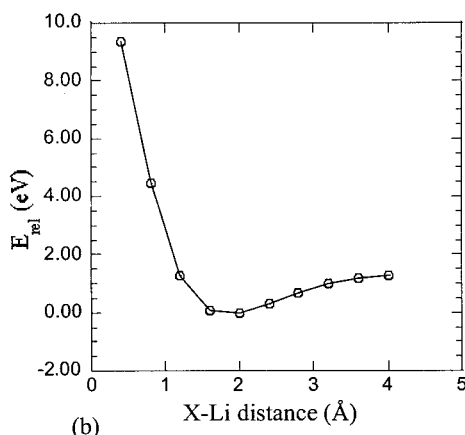
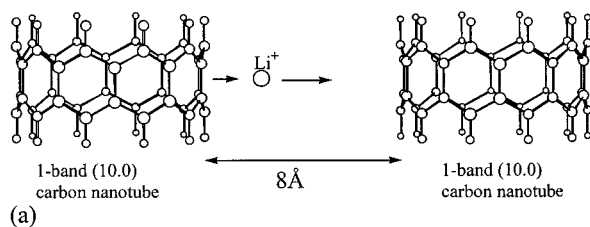


Figure 7. Model of tube bundle (a), and variation of energies (HF/3-21G) by moving lithium ion between two 1-band tubes (b).

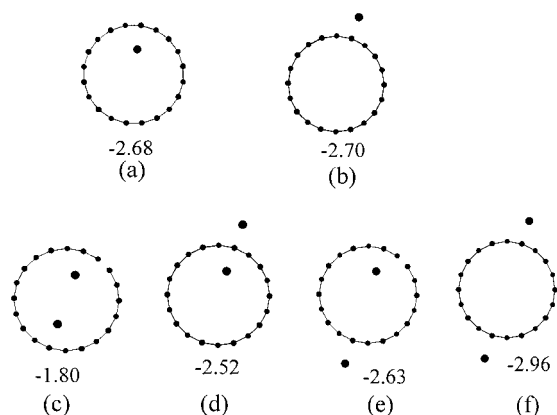


Figure 8. HF/3-21G optimized structures and binding energies (in eV) of different isomers of one (a and b) and two Li^+ (c–f) ions at 1-band nanotube.

Two Li^+ in 1-Band Tube. Both the model and the actual tube calculations suggest that the lithium ion prefers positions both inside and outside of the tube, with approximately equal energy. The equilibrium distance of 1.876 Å (inside as shown in Figure 8a) and 1.934 Å (outside in Figure 8b) refer to minima in the model calculations. Several combinations of inside and outside positions for two Li^+ in 1-band tube were considered, optimizing the distance between the cation and the wall of the tube. The electronic binding energy (ΔE) of the two ions to the tube strongly depends on the positions of those ions. The least stable ΔE value (−1.80 eV) is found when both the ions are inside the tube (Figure 8c) at a distance of 1.934 Å from the wall. This energy is substantially lower compared to the single cation systems. However, the stability of the dication system is enhanced if one Li^+ is moved outside. When both cations are attached to the same hexagon, one inside and another outside of the tube as shown in Figure 8d (as Li_2C_6 composition), the binding energy increases to −2.52 eV. More stable (by 0.11 eV) is the isomer where the second Li^+ occupies the outside position on the opposite side of the tube (Figure 8e). Most stable of all is the situation wherein both cations are outside, as in

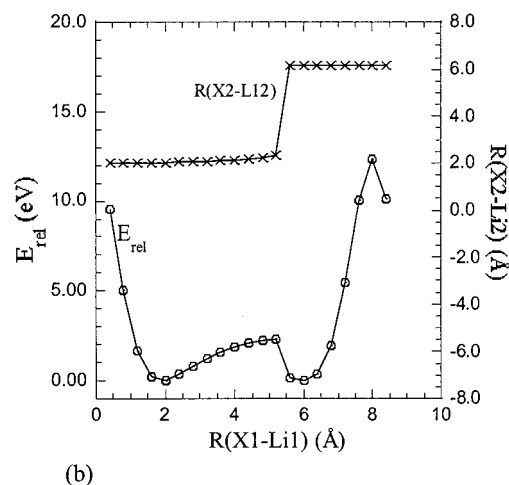
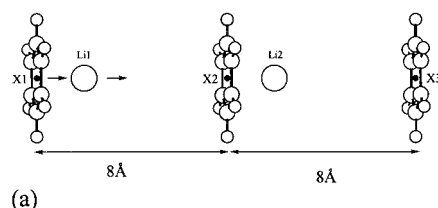


Figure 9. Three benzene and two lithium ions model (a), and variation of energies (HF/6-31G*) and distance between second lithium (Li_2) and center of middle ring (X_2) by moving first ion (Li_1) from the center (X_1) of the leftmost ring.

Figure 8f. This value is higher than the single cation system. Thus, it seems during intercalation process incoming ions occupy both inside and outside positions at a distance of 1.8 to 2.0 Å from the wall of the tube, with greater preference to external regions of the tubes.

In this and previous sections, it was found that results obtained from the simple 6-ring model are in good agreement with those of the actual tubes with no structural defects. From this finding, we believe our other ring models such as 5R and 7R will also provide reasonable energetic information about the lithium ion insertion process when other than hexagons are present in the tube, such as pentagon-hexagon defects, tube junctions or bent tubes, and cap regions of the closed tubes.

Multiwall Nanotube Model. The presence of multiple lithium ions in multiwall nanotubes is modeled by Figure 9a. These three 6-rings represent walls of three layers of a multiwall carbon nanotubes with inter-tube distance of 8 Å, along with two lithium ions. The energy obtained by moving first Li^+ (Li_1 in Figure 9a) from the wall of the leftmost 6R toward the center (X_2) of the middle ring is shown in Figure 9b. The position of the second ion (Li_2) is relaxed to move freely and respond to the motion of the first Li^+ (Li_1).

Besides the relative energy, the variation in the distance ($R(\text{X}_2-\text{Li}_2)$) from the center of the second ring to the second lithium ion is also reported in Figure 9b. It can be seen that the $R(\text{X}_2-\text{Li}_2)$ distance is almost constant around 2 Å as the first Li^+ approaches X_2 . As Li_1 passes the middle point of two rings at 4 Å, the second lithium ion starts moving very slowly. It may be noted that at this distance, we would expect a maximum in the curve in the absence of the second cation. The energy goes up further as the first Li^+ approaches X_2 because of the motion of the second ion. Sharp changes in energy and in X_2-Li_2 distance take place as Li_1 crosses 5.2 Å from X_1 . After this point, the Li_2 shifts sharply to its second preferred position, i.e., 2 Å from the center (X_3) of the rightmost 6-ring. The energy drops to a minimum when both the ions are at their second

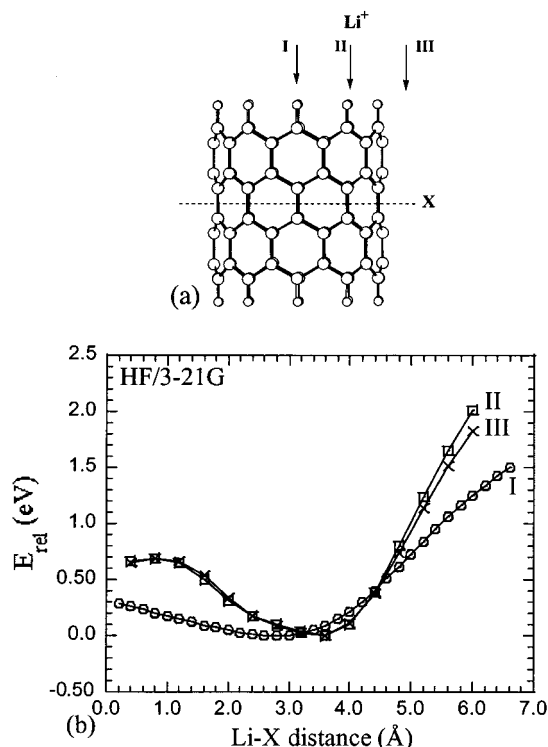


Figure 10. Insertion of Li^+ through the open end of 3-band tube (a), through the central axis (I) of the tube, 2.0 Å away from the wall: inside (II) and outside (III). Variation of energies by moving lithium ion along three different paths (b).

equilibrium position; Li1 and Li2 are 2 Å far from the middle and third 6-rings, respectively. Further movement of Li1 does not affect the position of Li2. However, the energy increases sharply as Li1 approaches closer to X2, and reaches a maximum at the wall as found in other models. It may be interesting to note that the barrier height of 2.3 eV in the present case is more than double that of two 6R and one Li^+ model in Figure 5b.

Open Tube Model. In the previous sections, we showed the energy profiles for insertion of lithium ions in closed tubes. The results clearly showed the difficulties of inserting Li^+ ion through the side wall or capped zone of a closed tube. In this section, we consider the diffusion of the cation through the open end of a 3-band tube. Three different paths for insertion are shown in Figure 10(a); along the central axis of the tube (path I), and 2.0 Å away from the wall, both inside (II) and outside (III). Variation of energy by moving lithium ion along these three paths is shown in Figure 10b. Relative energy curves clearly indicate that path II and III are equally favorable and different than path I. In all cases, the ion crosses through a minimum and a maximum at different locations of the tube. The barrier height for path I is significantly lower than II and III. In the former case Li^+ prefers to stay around 2.8 Å from X, i.e., 0.7 Å inside the tube from the open end. (Note that the tube length is around 7.0 Å when only carbon atoms are considered and about 9.0 Å with the inclusion of C–H bonds.) On the other hand, this distance is about 3.5 Å for other two paths, i.e., close to the mouth of the tube. From the present and previously discussed energetic information, it seems that lithium ions enter the tube through the central axis (path I) and may then spread inside the tube close to 2.0 Å from the wall.

Conclusion

In Li-rechargeable batteries, lithium ions get inside the carbon host (anode) during the charging process and are reversibly

released in the discharging process. Thus the barrier height of the intercalation process is a crucial factor in battery activity. It is also important to know the ions' positions and how easily they can move within the host materials.

A thorough theoretical investigation has been carried out using ab initio and DFT methods to understand the Li^+ insertion process into carbon nanotubes. A number of different structural arrangements of carbon nanotubes (CNTs) were considered. Several simple ring models have been used which represent single-wall closed tubes with structural defects, tube bundles, and multiwall tubes. To our knowledge this is the first systematic and extensive high level calculations on Li^+ @ CNTs.

Insertion of lithium ions through the side-wall or through the capped zone of the closed nanotubes seems energetically unfavorable unless there are structural defects. Even though Li^+ gets inside the tube in the electrochemical process, release of the ion during discharge process has to cross a very high barrier, depending on the ring size. The barrier height decreases from about 24.0 to 2.0 eV as the ring size of the wall increases from pentagon to octagon. The electronic binding energies of the cation at its equilibrium distance also decrease as the ring gets larger. For example, the binding energy drops from 2.2 to 1.1 eV as the ring size increases from pentagon to octagon. The equilibrium distance of the cation from the wall also decreases with ring size. For a nanotube with all hexagons, lithium ion prefers a distance around 1.9 Å from the wall of the tube. This distance is quite independent of the location of the ion, i.e., inside or outside of the single-wall tube, within a bundle of tubes or in a multiwall tube. Thus, it seems that ions outside the tubes may more easily take part in battery activities.

When a lithium ion moves from one wall to the other wall, it also crosses a low barrier at the center of a single-wall tube, or midpoint of two tubes in a bundle or the layers of a multiwall tube. This barrier height increases with enlarging diameter, or interlayer distance, or interstitial spacing of the tubes. Distances around 4 Å result in a single well potential.

Although lithium ion prefers sites both inside and outside of a tube, the outside position may be slightly more favorable. When two lithium ions are considered in a single-wall tube, the binding energy strongly depends on the ions' positions. The most stable configuration is the one where both ions are outside the tube; and the binding energy is higher than for the single cation system.

References and Notes

- (1) *Lithium Batteries*; Surampudi, S., Marsh, R., Eds.; The Electrochemical Society, Inc.: New Jersey, 1998; Vol. 98–16.
- (2) *Handbook of Battery Materials*; Besenhard, J. O., Ed.; Wiley-VCH: Weinheim, 1999.
- (3) Levy, S.; Bro, P. *Battery Hazards and Accidental Prevention*; Plenum Press: New York, 1994.
- (4) Murphy, D. W.; Carides, J. N. *J. Electrochem. Soc.* **1979**, *126*, 349–351.
- (5) Lazzari, M.; Scrosati, B. *J. Electrochem. Soc.* **1980**, *127*, 773–774.
- (6) Auburn, J. J.; Barberio, Y. L. *J. Electrochem. Soc.* **1987**, *134*, 638–640.
- (7) Nagaura, T.; Tozawa, K. *Prog. Batt. Solar Cells* **1990**, *9*, 209.
- (8) Dahn, J. R.; Sleigh, A. K.; Shi, H.; Way, B. M.; Weydanz, W. J.; Reimers, J. N.; Zhong, Q.; von Sacken, U. In *Lithium Batteries: New Materials, Developments, and Perspectives*; Pistoia, G., Ed.; Elsevier: Amsterdam, 1994; p 1.
- (9) Guyomard, D.; Tarascon, J. M. *J. Electrochem. Soc.* **1992**, *139*, 937–.
- (10) Flandrois, S.; Simon, B. *Carbon* **1999**, *37*, 165–180.
- (11) Endo, M.; Kim, C.; Nishimura, K.; Fujino, T.; Miyashita, K. *Carbon* **2000**, *38*, 183–197.
- (12) Dahn, J. R.; Zheng, T.; Liu, Y.; Xue, J. S. *Science* **1995**, *270*, 590–593.
- (13) Sato, K.; Noguchi, M.; Demachi, A.; Oki, N.; Endo, M. *Science* **1994**, *264*, 556–558.

- (14) Gong, J.; Wu, H.; Yang, Q. *Carbon* **1999**, *37*, 1409–1416.
- (15) Ryu, K. S.; Kim, K. M.; Kang, S.-G.; Lee, G. J.; Joo, J.; Chang, S. H. *Synth. Metals* **2000**, *110*, 213–217.
- (16) Bindra, C.; Nalimova, V. A.; Sklovsky, D. E.; Benes, Z.; Fischer, J. E. *J. Electrochem. Soc.* **1998**, *145*, 2377–2380.
- (17) Mordkovich, V. Z. *Synthetic Maters* **1996**, *80*, 243–247.
- (18) Nalimova, V. A.; Guerard, D.; Sklovsky, D. E.; Cox, D. *J. Phys. Chem. Solids* **1996**, *57*, 771–774.
- (19) Iijima, S. *Nature* **1991**, *354*, 56–58.
- (20) Dresselhaus, M. S.; Dresselhaus, G.; Eklunf, P. C. *Science of Fullerenes and Carbon Nanotubes*; Academic Press: New York, 1996.
- (21) *Carbon Nanotubes, Preparation and Properties*; Ebbesen, T. W., Ed.; CRC Press: New York, 1997.
- (22) Ajayan, P. M. *Chem. Rev.* **1999**, *99*, 1787–1799.
- (23) Harris, P. J. F. *Carbon Nanotubes and Related Structures, New Materials for the Twenty-First Century*; University Press: Cambridge, 1999.
- (24) *Fullerenes and Fullerene Nanostructures*; Kuzmany, H.; Fink, J.; Mehring, M.; Roth, S., Eds.; World Scientific: Singapore, 1996.
- (25) Saito, R.; Dresselhaus, G.; Dresselhaus, M. S. *Physical Properties of Carbon Nanotubes*; Imperial College Press: London, 1999.
- (26) Nalimova, V. A.; Sklovsky, D. E.; Bondarenko, G. N.; Alvergnat-Gaucher, H.; Bonnamy, S.; Beguin, F. *Synth. Metals* **1997**, *88*, 89–93.
- (27) Gao, B.; Kleinhammes, A.; Tang, X. P.; Bower, C.; Fleming, L.; Wu, Y.; Zhou, O. *Chem. Phys. Lett.* **1999**, *307*, 153–157.
- (28) Maurin, G.; Bousquet, C.; Henn, F.; Bernier, P.; Almairac, R.; Simon, B. *Chem. Phys. Lett.* **1999**, *312*, 14–18.
- (29) Frackowiak, E.; Gautier, S.; Gaucher, H.; Bonnamy, S.; Beguin, F. *Carbon* **1999**, *61*, 1–69.
- (30) Zhao, J.; Buldum, A.; Han, Jie.; Lu, J. P. *Phys. Rev. Lett.* **2000**, *85*, 1706–1709.
- (31) Gao, B.; Bower, C.; Lorentzen, J. D.; Fleming, L.; Kleinhammes, A.; Tang, X. P.; McNeil, L. E.; Wu, Y.; Zhou, O. *Chem. Phys. Lett.* **2000**, *327*, 69–75.
- (32) Frisch, M. J.; Trucks, H. B.; Schlegel, G. W.; Scuseria, G. E.; M. A. Robb, M. A.; Cheeseman, J. R.; Zakrzewski, V. G.; Montgomery, J., J. A.; Stratmann, R. E.; Burant, J. C.; Dapprich, S.; Millam, J. M.; Daniels, A. D.; Kudin, K. N.; Strain, M. C.; Farkas, O.; Tomasi, J.; Barone, V.; Cossi, M.; Cammi, R.; Mennucci, B.; Pomelli, C.; Adamo, C.; Clifford, S.; Ochterski, J.; Petersson, G. A.; Ayala, P. Y.; Cui, Q.; Morokuma, K.; Malick, D. K.; Rabuck, A. D.; Raghavachari, K.; Foresman, J. B.; Cioslowski, J.; Ortiz, J. V.; Baboul, A. G.; Stefanov, B. B.; Liu, G.; Liashenko, A.; Piskorz, P.; Komaromi, I.; Gomperts, R.; Martin, R. L.; Fox, D. J.; Keith, T.; Al-Laham, M. A.; Peng, C. Y.; Nanayakkara, A.; Gonzalez, C.; Challacombe, M.; Gill, P. M. W.; Johnson, B.; Chen, W.; Wong, M. W.; Andres, J. L.; Gonzalez, C.; Head-Gordon, M.; Replogle, E. S.; Pople, J. A. *Gaussian98, Rev. A7* **1998**, Gaussian, Inc., Pittsburgh, PA.
- (33) Feller, D.; Dixon, D. A.; Nicholas, J. B. *J. Phys. Chem. A* **2000**, *104*, 11 414–11 419.
- (34) Tsuzuki, T.; Yoshida, M.; Uchimar, T.; Mikami, M. *J. Phys. Chem. A* **2001**, *105*, 769–773.
- (35) Amicangelo, J. C.; Armentrout, P. B. *J. Phys. Chem. A* **2000**, *104*, 11 420–11 432.
- (36) Kar, T.; Ponc, R.; Sannigrah, A. B. *J. Phys. Chem. A* **2001**, *105*, 7737–7744.
- (37) Lammertsma, K.; Ohwada, T. *J. Am. Chem. Soc.* **1996**, *118*, 7247–7254.